Archimedean Spiral-Based Intercept Angle Guidance

Twinkle Tripathy* and Tal Shima†
Technion—Israel Institute of Technology, 3200003 Haifa, Israel

DOI: 10.2514/1.G004016

This paper focuses on designing an intercept angle guidance law for the planar interception of a stationary target. The underlying geometrical rule is based on an Archimedean spiral, which allows a pursuer to enforce a desired intercept angle or time by generating an appropriate spiral trajectory. An inherent advantage of using the proposed geometrical rule is that the required lateral acceleration to ensure interception is bounded throughout the engagement. The applicability of the geometrical rule is also analyzed against nonmaneuvering moving targets. The geometrical rule is implemented using a sliding-mode control-based nonlinear and robust guidance law. Using the proposed guidance law, the desired intercept angle is achieved in finite time. The theoretical results are validated through numerical simulations. The interception of the target with a specified intercept angle from different initial conditions and with various intercept angles from a given initial condition are shown. The robustness of the controller against disturbances and heading errors is also evaluated.

Nomenclature

a	=	Archimedean spiral parameter, m/rad
a_P	=	acceleration of the pursuer, m/s^2
$a_{P_{\text{eq}}}$	=	equivalent controller, m/s^2
$a_{P_{\text{un}}}$	=	uncertainty controller, m/s^2
I	=	interception point
N	=	gain for proportional navigation
P	=	pursuer notation
r_P	=	distance of the pursuer from the target
T	=	target notation
T_f	=	reachability time, s
t_f	=	final time, s
ν	=	speed ratio between the target and the pursuer
v_P	=	speed of the pursuer, m/s
v_T	=	speed of the target, m/s
v_r	=	rate of change of r_P, m/s
v_λ	=	rate of change of λ_P, rad/s
V	=	Lyapunov function
w	=	matched uncertainty in the input, m/s^2
(x_P, y_P)	=	position coordinate of the pursuer in Cartesian coordinate system, m
β	=	gain to drive the system to the sliding surface
γ_f	=	γ_P at interception, rad
γ_P	=	heading angle of the pursuer, rad
γ_T	=	heading angle of the target, rad
Δ	=	bound of the uncertainty in the time rate of change of the sliding variable, m/s^2
δ_P	=	lead angle of the pursuer, rad
δ_T	=	lead angle of the target, rad
η	=	gain of the uncertainty controller
κ	=	curvature of a curve, 1/m
λ_P	=	line-of-sight angle, rad
ξ_P	=	intercept angle, rad
σ	=	sliding variable, rad

I. Introduction

INTERCEPTION of a target at specific impact angles can enhance the effectiveness of a pursuer. For example, it can lead to a reduced warhead and less collateral damage, and it can facilitate an improved penetration. A vast variety of guidance laws are explored in the literature that allow a pursuer to enforce an intercept angle.

To begin with, classical guidance laws that implement the geometrical rules of pure pursuit and deviated pure pursuit (DPP) can be used to enforce a desired impact angle [1]. In pure pursuit, the velocity vector of the pursuer is directed towards the target, resulting in a tail-chase scenario. In DPP, the velocity vector of the pursuer maintains a constant lead angle from the line of sight (LOS) vector. By varying the lead angle, different intercept angles can be achieved. Another guidance law is proposed in [2], wherein Kim and Kim use a Lyapunov-based controller to minimize the error between the velocity vector and the LOS vector for stationary targets. To attack a target from a predefined direction, the guidance law is designed with intercept angle constraints at the final phase. In [3], Livermore and Shima implement DPP for a nonmaneuvering target using linear quadratic optimal control theory that allows a user to enforce either a desired impact time or angle.

One of the most remarkable guidance laws is proportional navigation guidance (PNG). A major advantage of PNG is that it requires zero control effort once the collision triangle is achieved. But, in general, PNG does not enforce a specific impact angle. However, it can be modified such that, along with interception, the additional constraint of an impact angle can also be attained. For the case of stationary targets, Lee et al. propose a guidance law composed of a PNG command and a function of an error term corresponding to the impact angle [4]. For nonmaneuvering targets, Ratnoo and Ghose propose two-stage PNG laws in [5,6] to intercept a target at desired impact angles. In the first stage, the guidance law orients the trajectory of the pursuer by using PNG with the navigation constant $N < 2$, which is later switched to $N > 2$ in the second stage to achieve the desired impact angle with a bounded terminal lateral acceleration.

An alternate approach is to consider small deviations from the collision triangle and obtain a linearized model of the engagement. Based on this linearized engagement model, optimal control and differential game theory can be used to design guidance laws that enforce an impact angle. When there is a large deviation from the collision triangle, the linearization does not hold. This problem is then overcome by linearizing the engagement model iteratively and solving the optimal control problem in each iteration. One of the earliest works [7] in this area deals with a terminal guidance law for a reentry vehicle with attitude constraints. Kim and Grider obtain the guidance law by formulating the problem as a linear-quadratic control problem with terminal constraints on the impact angle. Extending this approach for a pursuer with first-order dynamics, Ryoo et al. propose an optimal guidance law with an impact angle constraint in [8]. The aforementioned guidance laws use perfect information and lag-free dynamics of the target maneuver. While overcoming this limitation, Shaferman and Shima use differential game theory to obtain a guidance law with an intercept angle constraint in [9].

Received 6 August 2018; revision received 8 October 2018; accepted for publication 9 October 2018; published online 18 December 2018.

*Postdoctorate Fellow, Faculty of Aerospace Engineering; twinkle@technion.ac.il.

†Professor, Faculty of Aerospace Engineering; tal.shima@technion.ac.il. Associate Fellow AIAA.

The design of guidance laws that allow a pursuer to achieve a desired impact angle has also been pursued by using nonlinear control theory techniques like sliding-mode control [10]. In [11], Shima proposes a sliding-mode-based controller to achieve a desired intercept angle by maintaining a prespecified angle with respect to the target velocity vector. Rao and Ghose propose a second-order sliding-mode controller in [12] to guarantee a desired impact angle for the interception of a nonmaneuvering target. A sliding-mode control-based guidance law is designed by Harl and Balakrishnan in [13] that achieves not only a desired impact angle but also an impact time. In [14], Zhang et al. use the concept of finite time stability to design an intercept angle guidance law such that the error term associated with the sliding variable is forced to zero in finite time. Kumar et al. design a terminal sliding-mode control-based guidance law in [15] to enforce a desired impact angle that can be used against stationary, nonmaneuvering, and maneuvering targets. The authors improve upon the guidance law in [16] by proposing a nonsingular sliding-mode-based controller that overcomes the issue of a possible singularity resulting from small errors.

Geometrical rules inspired from mathematical curves have also been employed in the literature to achieve desired impact angles. Guidance laws implementing these geometrical rules shape the pursuer's trajectory to match the chosen mathematical curve. The properties of the curves are then adjusted such that desired specifications of lateral acceleration, smoothness, etc., can be enforced. In [17], Manchester and Savkin generate a circular trajectory by using the information of approach angles. The proposed guidance law achieves a desired impact angle without using the information of the range to the target. The mathematical principle of inscribed angles is used by Tsalik and Shima to design a guidance law in [18] to drive the pursuer along a circular trajectory to a target. The proposed guidance law is a three-point law. It achieves the desired impact angles by constraining the pursuer's trajectory to specific circular arcs by varying only the inscribed angle. In [19], the authors extend their work for the case of moving targets. Another three-point guidance law is proposed in [20] by Livermore et al., in which the trajectory of the pursuer follows an elliptical path. This guidance law can impose a launch angle along with enforcing desired impact angle and time for a stationary target.

The current work presents a geometrical rule based on the simple mathematical curve of a spiral. The motivation for the work is derived from the classical geometrical rule of DPP. Although DPP can enforce a desired impact angle, it suffers from the requirement of very large terminal lateral acceleration for the interception of stationary targets. This renders its implementation practically impossible. To overcome this problem, we propose a geometrical rule designed using an Archimedean spiral. Based on the properties of the spiral, we prove that the resulting lateral acceleration of the pursuer is bounded throughout the engagement. Furthermore, the mathematical properties of the curve can be modified to enforce impact angle or time constraints at target capture. We also discuss the conditions to intercept a target moving in a straight-line path using the proposed geometrical rule. The implementation of the geometrical rule is carried out using a sliding-mode controller, which is a nonlinear robust controller that rejects the bounded disturbances appearing in the system. In addition to it, the implementation requires only angular information. Another advantage of the guidance law is that it is not designed assuming near-collision-course conditions and, hence, is valid throughout the engagement.

The paper is organized as follows. Section II formulates the problem of planar interception of a stationary target. In Sec. III, the Archimedean spiral-based geometrical rule is presented. The performance of the proposed geometrical rule in terms of target capturability is elaborated in Sec. IV. Section V discusses the lateral acceleration requirements for the proposed geometrical rule. For the implementation of the geometrical rule, a sliding-mode controller is proposed in Sec. VI. In Sec. VII, we discuss the performance of the proposed geometrical rule against a nonmaneuvering and a nonstationary target. The validation of the theoretical results is carried out using numerical simulations in Sec. VIII. Finally, Sec. IX concludes the paper.

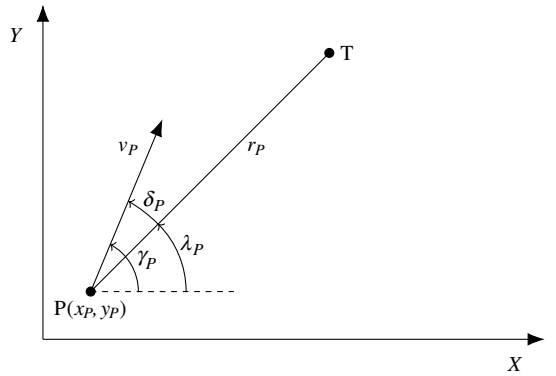

Fig. 1 Planar geometry between the pursuer and the target.

II. Problem Description

The paper focuses on designing a guidance law for the interception of a stationary target such that the lateral acceleration of the pursuer is bounded throughout the engagement. A planar engagement between the target T and the pursuer P is considered. In the inertial Cartesian coordinate system, the nonlinear engagement kinematics are as follows:

$$\begin{aligned}\dot{x}_P &= v_P \cos\gamma_P \\ \dot{y}_P &= v_P \sin\gamma_P \\ \dot{\gamma}_P &= a_P/v_P\end{aligned} \tag{1}$$

where (x_P, y_P) denotes the position coordinates of the pursuer, and a_P is the lateral acceleration perpendicular to its velocity. The pursuer is assumed to be moving at a constant speed v_P with a heading angle γ_P. The planar engagement geometry between the pursuer and the target is shown in Fig. 1, where the distance and line-of-sight angle between P and T are denoted by r_P and λ_P, respectively, satisfying

$$\begin{aligned}\dot{r}_P &= -v_P \cos(\gamma_P - \lambda_P) = -v_P \cos\delta_P \\ r_P\dot{\lambda}_P &= -v_P \sin(\gamma_P - \lambda_P) = -v_P \sin\delta_P\end{aligned} \tag{2}$$

δ_P is called the lead angle, which is the angle between the velocity vector of the pursuer and the line of sight between the target and the pursuer.

With the preceding equations of motion of the pursuer, the objective of the present work is to design a_P such that it is always bounded and interception is achieved with a desired impact angle. To achieve this, a new geometrical rule is proposed in the following section.

III. New Geometrical Rule

In this section, we propose a geometrical rule inspired from the unique mathematical properties of an Archimedean spiral.

A. Motivation

This work derives its motivation from the geometrical rule of DPP, the details of which can be found in [1]. In DPP, the pursuer tries to maintain its velocity vector at a prespecified lead angle from the line of sight joining the pursuer and the target. When it comes to a stationary target, a major drawback associated with this geometrical rule is severe maneuver requirements toward interception. The trajectory of the pursuer trying to intercept a stationary target by using DPP [1] is given as follows:

$$r_P(\lambda_P) = r_{P0} \exp(-\lambda_P \cot\delta_P) \tag{3}$$

Equation (3) describes a logarithmic spiral. By the very nature of the curve, it approaches the origin spiraling its way inside infinitely many number of times. This causes the turn rates to be very high near the origin. For a pursuer following this trajectory, the lateral acceleration [1] reduces to

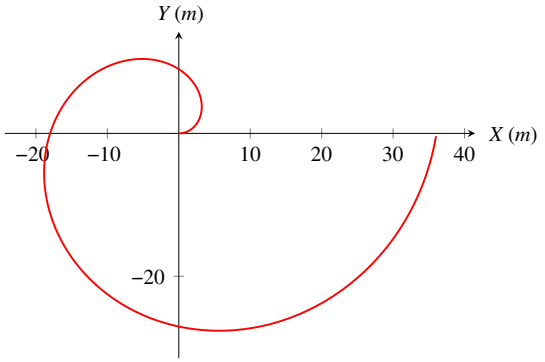

Fig. 2 Archimedean spiral.

$$a_P(\lambda_P) = \frac{v_P^2 \sin\delta_P}{r_P} \tag{4}$$

Given that v_P and δ_P are constant for DPP, it is evident from Eq. (4) that, as $r_P \to 0$, the lateral acceleration a_P shoots up to infinity. This adversely affects the implementability of the DPP geometrical rule against stationary targets. This creates the urge to look for geometrical rules that result in trajectories that can overcome this issue while still being generic enough to be implemented easily.

B. Archimedean Spiral-Based Geometrical Rule

Consider an Archimedean spiral defined in polar coordinates as follows:

$$r = a\lambda \tag{5}$$

where $a \in \mathbb{R}$ is a constant. Equation (5) results in the spiral shown in Fig. 2. The curvature of the spiral is $\kappa(\lambda) = (2+\lambda^2)/(a(1+\lambda^2)^{1.5})$. Hence, $\kappa = 2/a$ at $\lambda = 0$. Interestingly, this implies that the curve approaches origin with a zero intercept angle and a finite curvature for all values of a. To generate a spiral trajectory with a specific intercept angle ξ, Eq. (5) can be modified as follows:

$$r = a(\lambda - \xi) \tag{6}$$

With this knowledge, next we proceed to derive a geometrical rule to achieve a spiral governed by Eq. (6).

Theorem 1: For a pursuer with kinematics given by Eq. (1), an Archimedean spiral trajectory corresponds to the geometrical rule

$$\tan\delta_P = \lambda_P - \xi_P \tag{7}$$

such that the intercept angle is ξ_P.

Proof: For $r = r_P$, $\lambda = \lambda_P$, and $\xi = \xi_P$, the equation of an Archimedean spiral given in Eq. (6), is substituted in the kinematics [Eq. (2)] of the pursuer, which gives $-v_P\cos\delta_P = a(-v_P\sin\delta_P/r_P)$. Further simplification results in the geometrical rule $\tan\delta_P = \lambda_P - \xi_P$. □

IV. Capturability Region

This section presents the conditions for the interception of the target based on the initial coordinates of the pursuer.

To begin with, using the equations of motion in Eq. (2), we define v_r and v_λ as

$$v_\lambda = r_P\dot{\lambda}_P = -v_P\sin\delta_P \tag{8}$$

$$v_r = \dot{r}_P = -v_P\cos\delta_P \tag{9}$$

Squaring and adding Eqs. (8) and (9) gives

$$v_\lambda^2 + v_r^2 = v_P^2 \tag{10}$$

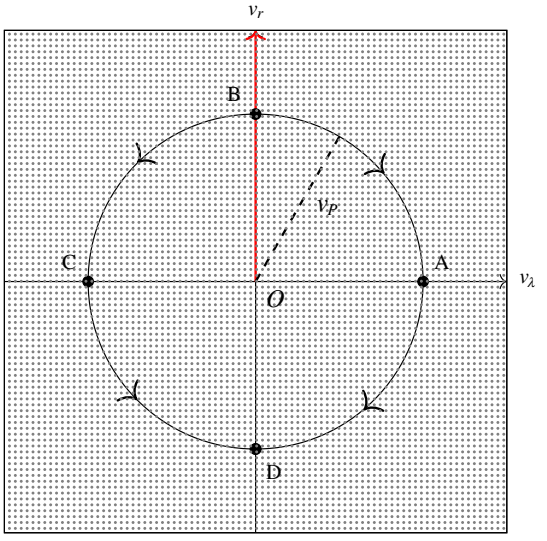

Fig. 3 Variation of v_r and v_λ.

This defines a circle of radius v_P centered at the origin. Now, we define a Cartesian frame of reference $V_\lambda - O - V_r$ with its origin at $\mathcal{O}(v_\lambda = 0, v_r = 0)$. In $V_\lambda - O - V_r$, Eq. (10) implies that the instantaneous values of v_r and v_λ always lie on a circle centered at the origin with radius v_P, as shown in Fig. 3.

The rates of change of v_λ and v_r are calculated using Eqs. (8) and (9) and evolve with time as given next:

$$\dot{v}_\lambda = -v_P\cos\delta_P\dot{\delta}_P = v_r\dot{\delta}_P \tag{11}$$

$$\dot{v}_r = v_P\sin\delta_P\dot{\delta}_P = -v_\lambda\dot{\delta}_P \tag{12}$$

The proposed geometrical rule is $\tan\delta_P = \lambda_P - \xi_P$. Differentiating and then rearranging, we get

$$\dot{\delta}_P = \cos^2\delta_P\dot{\lambda}_P \tag{13}$$

Substituting Eq. (13) in Eqs. (11) and (12), we obtain

$$\dot{v}_r = -v_\lambda^2\cos^2\delta_P/r_P \tag{14}$$

$$\dot{v}_\lambda = v_r v_\lambda\cos^2\delta_P/r_P \tag{15}$$

To understand how v_λ and v_r vary with time, we take a look at the circle of radius v_P plotted in Fig. 3. There are four points of significance associated with the circle, which we call the critical points. They are

$$A\text{: } (v_\lambda, v_r) = (v_P, 0) \tag{16}$$

$$B\text{: } (v_\lambda, v_r) = (0, v_P) \tag{17}$$

$$C\text{: } (v_\lambda, v_r) = (-v_P, 0) \tag{18}$$

$$D\text{: } (v_\lambda, v_r) = (0, -v_P) \tag{19}$$

The analysis that follows is along the same lines as given in [21]. At A and C, $v_\lambda \neq 0$ and $v_r = 0$. Because, due to Eq. (14), v_r decreases monotonically for $v_\lambda \neq 0$, the latter implies that v_r changes sign at these points. Hence, these points correspond to the points of closest approach where miss distance occurs in case the pursuer misses the target. At B and D, $v_\lambda = 0$, then $\dot{v}_r = \dot{v}_\lambda = 0$. It can be easily shown that the rest of the higher derivatives of v_λ and v_r also go to zero, implying that v_λ and v_r remain constant with time thereafter. At point B, $v_r > 0$. Thus, r_P keeps increasing while the line of sight does not rotate and the pursuer and the target move away from each other. The point of interest is D, where $v_r < 0$. Now, $v_\lambda = 0$ implies either $r_P = 0$

or $\dot{\lambda}_P = 0$. If $r_P = 0$, then the pursuer has already intercepted the target. When $\dot{\lambda}_P = 0$, the line of sight does not rotate with time. This means that r_P keeps reducing, and the pursuer and the target keep approaching each other until collision. Thus, if the instantaneous value of (v_λ, v_r) converges to D, then target capture is guaranteed.

Now, Eq. (14) shows that

$$\dot{v}_r < 0, \qquad \forall\ v_\lambda \in [-v_P, v_P] \setminus \{0\} \quad \text{and} \quad v_r \in (-v_P, v_P) \tag{20}$$

The sign of $\dot{v}_\lambda$ depends on v_r and v_λ, as shown next:

$$\frac{\dot{v}_\lambda}{|\dot{v}_\lambda|} = \begin{cases} 1 & \text{if } v_\lambda \quad v_r > 0 \\ -1 & \text{if } v_\lambda \quad v_r < 0 \end{cases} \tag{21}$$

Combining Eqs. (20) and (21), we conclude that the instantaneous values of (v_λ, v_r) always move downward towards point D in the circle shown in Fig. 3, unless $v_r = v_P$. When $v_r = v_P$, the trajectory starts at point B, and the pursuer is driven away from the target thereafter. For every other initial condition, (v_λ, v_r) eventually reaches point D, and collision is guaranteed.

When v_P is specified, every point on the circle shown in Fig. 3 belongs to the capturability region, except point B, where $v_r = v_P$. Now, as v_P varies from $(0, \infty)$, B spans over the whole positive v_r axis. Thus, the capturability region becomes the entire (v_λ, v_r) plane, except the positive v_r axis, which is highlighted in red in Fig. 3. In the figure, the capturability region is shown as the area dotted in gray.

Target capture always occurs at point D, where $v_r = -v_P$. Using Eq. (11), $\delta_P = 0$ at the end of the engagement. Now, by the very definition of the geometrical rule, we have $\delta_P = \tan^{-1}(\lambda_P - \xi_P)$. Mathematically, inverse tangent is a multivalued function defined in the range $(n(\pi/2), n(\pi/2) + \pi)$ for integer values of n. In our case, we choose $n = -1$ to get $\delta_P \in (-\pi/2, \pi/2)$. This range is chosen because it is the only one containing $\delta_P = 0$, which necessarily occurs at target capture. Then, from Eq. (11), we get

$$v_r = -v_P \cos\delta_P < 0 \tag{22}$$

for all initial conditions r_{P_0} and λ_{P_0} where $\delta_{P_0} = \tan^{-1}(\lambda_{P_0} - \xi_P)$ such that the geometrical rule holds. This narrows down the capturability region to the negative v_r plane. As we already know, for target capture, the trajectory of the pursuer ends at point D, where $(v_\lambda, v_r) = (0, -v_P)$. Depending on the initial value of λ_P, two interesting cases arise when the trajectory reaches there which, are discussed next.

$\lambda_{P_0} = \xi_P$: In this case, $\tan\delta_0 = 0$, which implies $\delta_0 = 0$. $\delta_0 = \pi$ is not an option so that it corresponds to point D and not B. Then, $v_r = -v_P$ and $v_\lambda = 0$ hold from the start of the engagement. This results in the well-known collision triangle as $\dot{\lambda}_P = 0$. Here, it reduces to the line joining the initial coordinates of the pursuer and the target, given by $r_P(t) = -v_P t + r_{P_0}$ for all time $t \geq 0$.

Then, the final time reduces to $t_f = r_0/v_P$. We consider the scenario given by: $v_P = 500$, $r_{P_0} = 1000$, $\lambda_{P_0} = 7\pi/4$, $\xi_P = 7\pi/4$, and $\delta_{P_0} = 0$. The trajectory of the pursuer in this situation is shown in Fig. 4a, where the circle and the asterisk denote the target and the initial position of the pursuer, respectively. The variations of r_P and λ_P are shown in Figs. 4b and 4c, respectively.

$\lambda_{P_0} \neq \xi_P$: Here, $\tan\delta_0 \neq 0$, which implies $v_{r_0} \neq -v_P$. The trajectory does not start at the point D. But as discussed earlier in this section, it is driven always to D under the proposed geometrical rule. At D, $v_\lambda = 0$, which implies $\delta_P = 0$ and $\lambda_P = \xi_P$.

Now, the proposed geometrical rule is derived from the Archimedean spiral. Hence, the system kinematics is driven such that the trajectory is an Archimedean spiral for all time $t \geq 0$ defined by the equation $r_P = a(\lambda_P - \xi_P)$ where $a = (r_0/\lambda_0 - \xi_P)$. Then, the desired intercept angle is achieved at target capture as $r_P = 0$ when $\lambda_P = \xi_P$. This can be clearly seen in Fig. 5, which is simulated for $v_P = 500$, $r_{P_0} = 1000$, $\lambda_{P_0} = 5\pi/4$, $\xi_P = 7\pi/4$, and $\delta_{P_0} = -1.004$. The trajectory of the pursuer is shown in Fig. 5a, where the circle and the asterisk represent the target and the initial position of the pursuer,

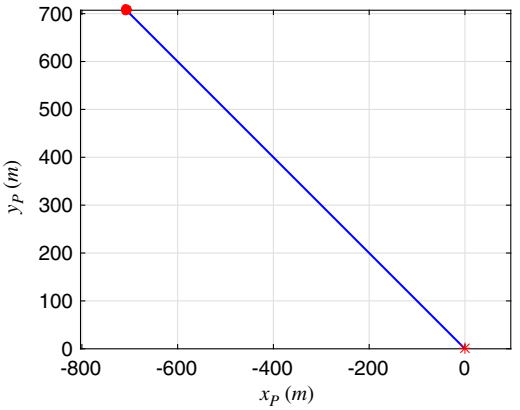

a) Trajectory of the pursuer

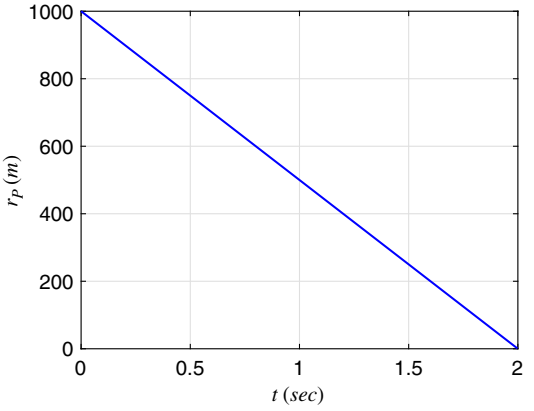

b) Variation of r_P with time

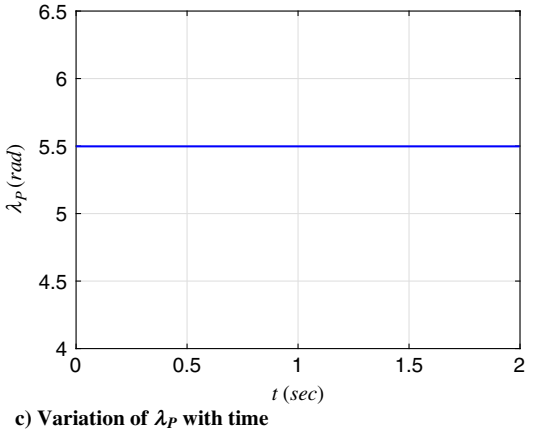

c) Variation of λ_P with time

Fig. 4 Target capture for $\lambda_{P_0} = \xi_P$.

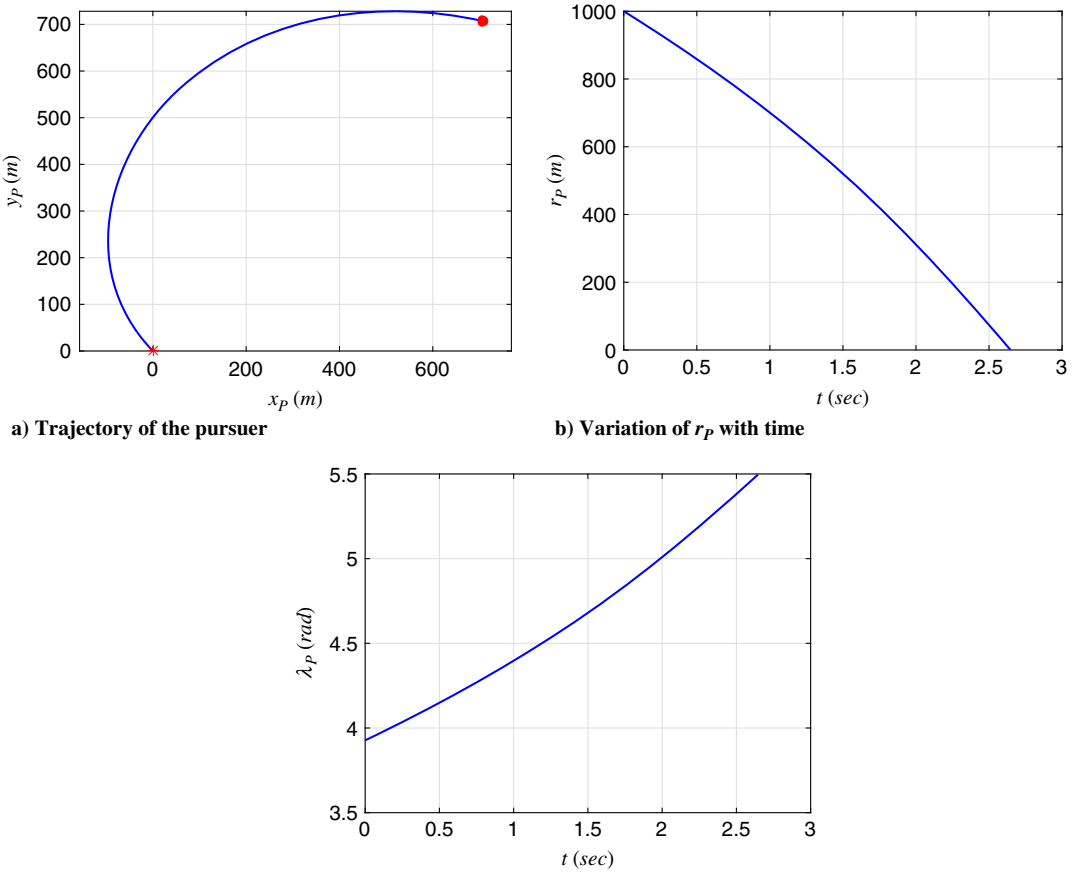

a) Trajectory of the pursuer

b) Variation of r_P with time

c) Variation of λ_P with time

Fig. 5 Target capture for $\lambda_{P_0} \neq \xi_P$.

respectively. Figures 5b and 5c show the variation of r_P and λ_P, respectively.

A. Behavior of the Engagement Parameters

In this subsection, we discuss the variation of engagement parameters with respect to time.

r_P: Equation (20) shows that $\dot{v}_r < 0$ for all time $t \geq 0$. Moreover, Eq. (22) shows that $v_r < 0$ throughout the engagement. Thus, r_P reduces to zero monotonically. This can be seen in Fig. 5b where the monotonicity of r_P holds for the given engagement scenario.

λ_P: From Eq. (6), we get $\dot{\lambda}_P = v_r/a$, where $a = r_0/(\lambda_{P_0} - \xi_P)$. Further trigonometric substitutions give $\dot{\lambda}_P = -\text{sign}(a)(v_P/\sqrt{r_P^2 + a^2})$. At t_f, $\dot{\lambda}_P = -\text{sign}(a)(v_P/|a|)$. For $a > 0$, $\dot{\lambda}_P$ decreases monotonically to $\dot{\lambda}_P|_{t=t_f} = -v_P/a$, else it increases until $\dot{\lambda}_P|_{t=t_f} = v_P/|a|$ is reached. For the scenario presented in Fig. 5, $a = -636.62$; hence, λ_P increases monotonically as shown in Fig. 5c.

δ_P: Equation (13) shows that δ_P varies in the same manner as λ_P. The only difference is that δ_P converges to zero at t_f for all values of a, v_{r_0}, and ξ_P.

Because $\gamma_P = \delta_P + \lambda_P$, γ_P varies in accordance with λ_P. Further, $\delta_P = 0$ at t_f which gives $\gamma_P|_{t=t_f} = \gamma_f = \xi_P$. Thus, the desired intercept angle is always achieved at target capture.

B. Impact Time

The equation of an Archimedean spiral is given in Eq. (7). The arc length of this spiral is $s(\lambda_P) = (1/2)a((\lambda_P - \xi_P)\sqrt{1 + (\lambda_P - \xi_P)^2} + \sinh^{-1}(\lambda_P - \xi_P))$ [22]. For a constant speed v_P, the impact time is given by using Eq. (7) as

$$t_f = \frac{1}{2v_P}\frac{r_{P_0}}{\lambda_{P_0} - \xi_P}\left((\lambda_{P_0} - \xi_P)\sqrt{1 + (\lambda_{P_0} - \xi_P)^2} + \sinh^{-1}(\lambda_{P_0} - \xi_P)\right) \tag{23}$$

Hence, the proposed geometrical rule can also enforce an impact time by suitable choice of the spiral parameter a or the initial conditions r_{P_0} and λ_{P_0}.

The impact angle is also related to the spiral parameter and initial conditions as shown below:

$$\xi_P = \lambda_{P_0} - \frac{r_{P_0}}{a} = \lambda_{P_0} - \tan\delta_{P_0} \tag{24}$$

From Eqs. (23) and (24), it is evident that, by using the proposed geometrical rule, both impact time and angle can be imposed on the trajectory of the pursuer. However, arbitrary values of t_f and ξ_P cannot be achieved simultaneously because they are dependent on the same parameters.

Thus, it is established that the geometrical rule not only ensures target capture but also achieves it with a desired intercept angle or time. Next, we discuss the variation of the lateral acceleration a_P during the engagement for different initial conditions and parameters of the proposed geometrical rule.

V. Bounds on Lateral Acceleration

Under the proposed geometrical rule, $\tan\delta_P = \lambda_P - \xi_P$, which gives $\dot{\delta}_P = \cos^2\delta_P\dot{\lambda}_P$. From the third equation in Eqs. (1), we know that $\dot{\gamma}_P = \dot{\delta}_P + \dot{\gamma}_P = (1 + \cos^2\delta_P)\dot{\lambda}_P$. Because $a_P = v_P\dot{\gamma}_P$, the lateral acceleration is then given by

$$a_P = v_P(1 + \cos^2\delta_P)\dot{\lambda}_P \tag{25}$$

This is equivalent to PNG with a varying gain $N = (1 + \cos^2\delta_P)$, such that $1 \leq N \leq 2$. As r_P tends to zero, it has been proved in the previous section that δ_P also tends to zero. Hence, at target capture, the guidance law behaves like PNG with $N = 2$.

The trajectory of the pursuer following PNG with $N = 2$ is circular with a constant lateral acceleration. Therefore, under the proposed geometrical rule, the lateral acceleration at target capture is always finite. Figure 6a shows the variation of the parameter N for the following initial conditions: $r_{P_0} = 1000$, $\lambda_{P_0} = 3\pi/4$, $\xi_P = \pi/4$, and $\delta_{P_0} = \pi/3$. It is evident that $N \to 2$ as $r_P \to 0$. Figure 6b shows the plot of the lateral acceleration, from which it is clear that a_P is finite.

Next, we calculate the bounds of a_P. In a Cartesian frame of reference, the curvature of any curve [23] is given by

$$\kappa = \frac{x'y'' - x''y'}{(x'^2 + y'^2)^{1.5}} \tag{26}$$

To find the behavior of the trajectory of the pursuer, we substitute the equations of motion from Eqs. (1) in Eq. (26) to obtain

$$\kappa = \frac{(v_P \cos\gamma_P)(\cos\gamma_P a_P) - (v_P \sin\gamma_P)(-\sin\gamma_P a_P)}{v_P^2 \cos^2\gamma_P + v_P^2 \sin^2\gamma_P} = \frac{a_P}{v_P} \tag{27}$$

This shows that, for a constant speed v_P, the kinematics of the pursuer drives the trajectory in such a manner that its curvature is a linear function of the lateral acceleration only.

The curvature [22] of an Archimedean spiral, as defined in Eq. (6), can be expressed as follows:

$$\kappa(\lambda_P) = \frac{2 + (\lambda_P - \xi_P)^2}{a(1 + (\lambda_P - \xi_P)^2)^{1.5}} \tag{28}$$

where $a = r_{P_0}/(\lambda_{P_0} - \xi_P)$. As a increases, the curvature of the spiral at any given λ_P reduces. This property can be exploited to design curves with curvatures lower than some specific values.

In Eq. (28), κ is strictly a function of λ_P because a and ξ_P are constants. To study the variation of κ with respect to λ_P, we look for the points of extrema in the curve. We start with the following:

$$\frac{d\kappa}{d\lambda_P} = -\frac{(\lambda_P - \xi_P)(1 + (\lambda_P - \xi_P)^2)^{0.5}(4 + (\lambda_P - \xi_P)^2)}{a(1 + (\lambda_P - \xi_P)^2)^3} \tag{29}$$

$(d\kappa/d\lambda_P) = 0$ gives $\lambda_P = \xi_P$, which is the only point at which an extremum occurs. To find whether the extremum is a maximum or a minimum, $\lambda_P = \xi_P$ is substituted in the second derivative, which gives

$$\left.\frac{d^2\kappa}{d\lambda_P^2}\right|_{\lambda_P = \xi_P} = -4$$

This implies that, for an Archimedean spiral, the curvature becomes maximum at $\lambda_P = \xi_P$ and is equal to

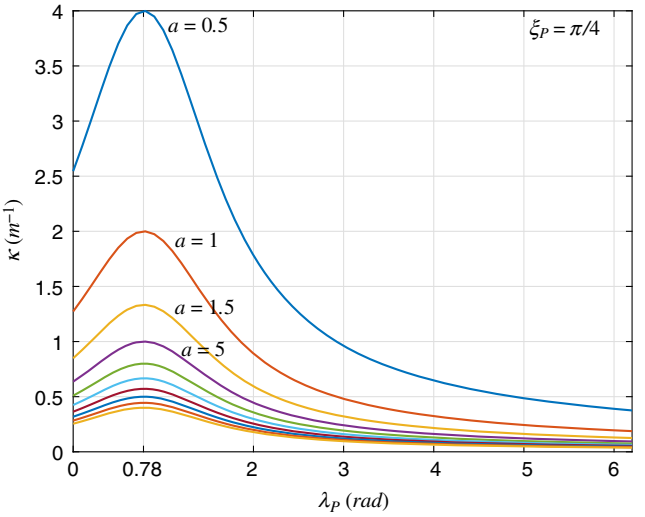

Fig. 7 Curvature of an Archimedean spiral.

$$\max(\kappa) = 2/a \tag{30}$$

The variation of κ with respect to λ_P is shown in Fig. 7 for $\xi_P = 0.78$ rad. As is evident in the figure, the maximum value of the curvature occurs at $\lambda_P = \xi_P$.

Now, substituting Eq. (27) in Eq. (28) gives

$$a_P = v_P \kappa = v_P \frac{2 + (\lambda_P - \xi_P)^2}{a(1 + (\lambda_P - \xi_P)^2)^{1.5}} \tag{31}$$

Because the lateral acceleration is a scalar function of the curvature, the former also has an extremum at $\lambda_P = \xi_P$. The maximum value of the lateral acceleration is calculated using Eqs. (30) and (31) and is given as follows:

$$\max(a_P) = \frac{2v_P}{a} \tag{32}$$

Let us assume that the maximum permissible lateral acceleration for the pursuer is denoted as $a_{P_{\max}}$. Any Archimedean spiral for which the initial distance to target r_{P_0}, the initial line-of-sight angle λ_{P_0}, and intercept angle ξ_P satisfy $a = \frac{r_{P_0}}{\lambda_{P_0} - \xi_P} \geq \frac{2v_P}{a_{P_{\max}}}$ can be chosen as the pursuer's trajectory. Such a value of a ensures that the required a_P does not exceed its maximum permissible value.

At interception, r_P tends to zero, and λ_P tends to ξ_P. Thus, from the preceding analysis, we infer that the maximum lateral acceleration is required at interception; nonetheless, it is bounded for all finite values

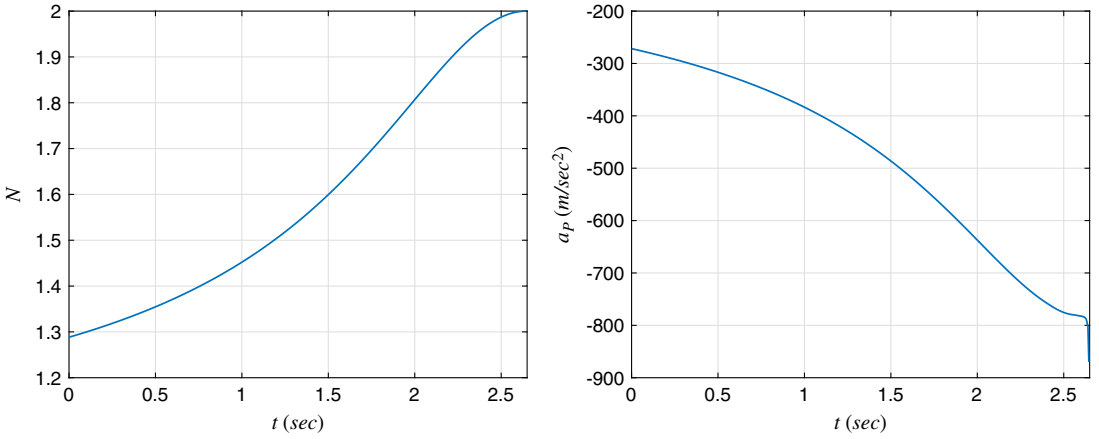

a) Variation of N **b) Variation of lateral acceleration**

Fig. 6 Equivalence to PNG.

of the parameter a. This makes the implementation of the geometrical rule feasible.

VI. Guidance Law

In this section, a sliding-mode controller is used to derive a guidance law [24] whose objective is to impose the geometrical rule in Eq. (7) on the system kinematics given in Eqs. (1). We assume that the system is corrupt with some external disturbances entering through the input channel arising from wind disturbances, process noise, etc., in which case the kinematics of the system in Eq. (2) becomes

$$\begin{aligned}\dot{r}_P &= -v_P\cos(\gamma_P-\lambda_P)\\ \dot{\lambda}_P &= -v_P\sin(\gamma_P-\lambda_P)/r_P\\ \dot{\gamma}_P &= (a_P+w)/v_P\end{aligned} \tag{33}$$

where w is an external disturbance that is a matched uncertainty to the system.

Sliding-Mode Controller: The geometrical rule in Eq. (7) commands a desired lead angle, denoted by ξ_P, with respect to the line-of-sight angle λ_P. Let the sliding surface be designed as

$$\sigma = \tan\delta_P - \lambda_P + \xi_P \tag{34}$$

The time derivative is computed to be $\dot{\sigma} = \sec^2\delta_P a_P/v_P + \sec^2\delta_P w/v_P + (1+\sec^2\delta_P)v_P\sin(\gamma_P-\lambda_P)/r_P$. Now, the sliding-mode controller consists of an equivalent component $a_{P_{\text{eq}}}$ and an uncertainty component $a_{P_{\text{un}}}$ [10] such that

$$a_P = a_{P\text{eq}} + a_{P\text{un}} \tag{35}$$

The equivalent controller ensures that the system is maintained on the sliding surface in the absence of disturbances. Thus, it is chosen as

$$\begin{aligned}a_{P\text{eq}} &= \frac{v_P}{\sec^2\delta_P}(1+\sec^2\delta_P)\dot{\lambda}_P\\ &= \frac{v_P}{\sec^2\delta_P}\left[-(1+\sec^2\delta_P)\frac{v_P\sin(\gamma_P-\lambda_P)}{r_P}\right]\end{aligned} \tag{36}$$

It is to be noted that, without any uncertainty, the system is driven towards the sliding surface with $a_P = a_{P\text{eq}}$. Now, the substitution of the equivalent controller in the expression of $\dot{\sigma}$ gives

$$\dot{\sigma} = \frac{\sec^2\delta_P}{v_P}(a_{P\text{un}} + w)$$

The uncertainty controller $a_{P\text{un}}$ is then chosen as

$$a_{P\text{un}} = -\beta\,\text{sgn}(\sigma) \tag{37}$$

such that $\beta > 0$. This gives $\dot{\sigma} = \sec^2\delta_P(-\beta\,\text{sgn}(\sigma)+w)/v_P$. To check the stability of the system, a candidate Lyapunov function $V = 0.5\sigma^2$ is considered. Then,

$$\begin{aligned}\dot{V} = \sigma\dot{\sigma} &= \sigma(-\beta\,\text{sgn}(\sigma)+w)\frac{\sec^2\delta_P}{v_P}\\ &\le -|\sigma|(\beta-|w|)\frac{\sec^2\delta_P}{v_P} \le -\eta V^{0.5}\end{aligned} \tag{38}$$

where $\eta > \sec^2\delta_P(\beta-|w|)/v_P > 0$, implying the bound on the gain as $\beta > \max(|w|)$.

It can be shown from Eq. (38) that the sliding surface is reached in finite time $T_f \le 2V^{0.5}(0)/\eta$. Once the sliding surface is reached, the geometrical rule holds thereafter. Then, the interception of the target can be guaranteed using the results of Sec. IV.

VII. Moving Targets

In this section, we analyze the performance of the proposed geometrical rule against a moving target. The target is assumed to be nonmaneuvering while moving in a straight line. Let the target speed be v_T. The heading angle and the lead angle of the target are denoted by γ_T and δ_T, respectively. The engagement geometry is shown in Fig. 8a. In this case, we show that the actual intercept angle of the pursuer, denoted by γ_f in Fig. 8b, is different from the desired intercept angle ξ_P. But the difference between γ_f and ξ_P is known beforehand and hence can be compensated.

The nonlinear engagement kinematics can be written as

$$v_r = \dot{r}_P = v_T\cos\delta_T - v_P\cos\delta_P \tag{39}$$

$$v_\lambda = r\dot{\lambda}_P = v_T\sin\delta_T - v_P\sin\delta_P \tag{40}$$

The time derivatives of the equations are given next:

$$\dot{v}_r = -v_T\sin\delta_T\dot{\delta}_T + v_P\sin\delta_P\dot{\delta}_P \tag{41}$$

$$\dot{v}_\lambda = v_T\cos\delta_T\dot{\delta}_T - v_P\cos\delta_P\dot{\delta}_P \tag{42}$$

Under the effect of the proposed geometrical rule, the equations of motion evolve as follows:

$$\dot{v}_r = -v_T\sin\delta_T(-\dot{\lambda}_P) + v_P\sin\delta_P(\cos^2\delta_P\dot{\lambda}_P) \tag{43}$$

$$\dot{v}_\lambda = v_T\cos\delta_T(-\dot{\lambda}_P) - v_P\cos\delta_P(\cos^2\delta_P\dot{\lambda}_P) \tag{44}$$

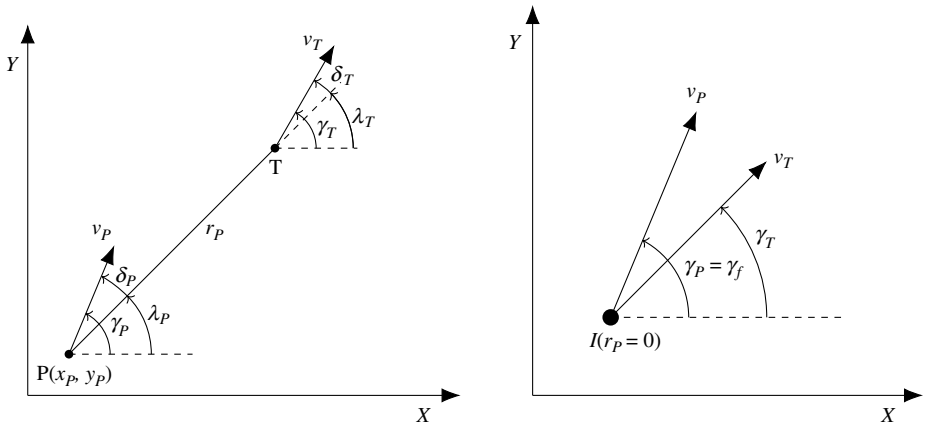

a) Planar geometry between the pursuer and the target

b) Actual intercept angle γ_f

Fig. 8 Moving target.

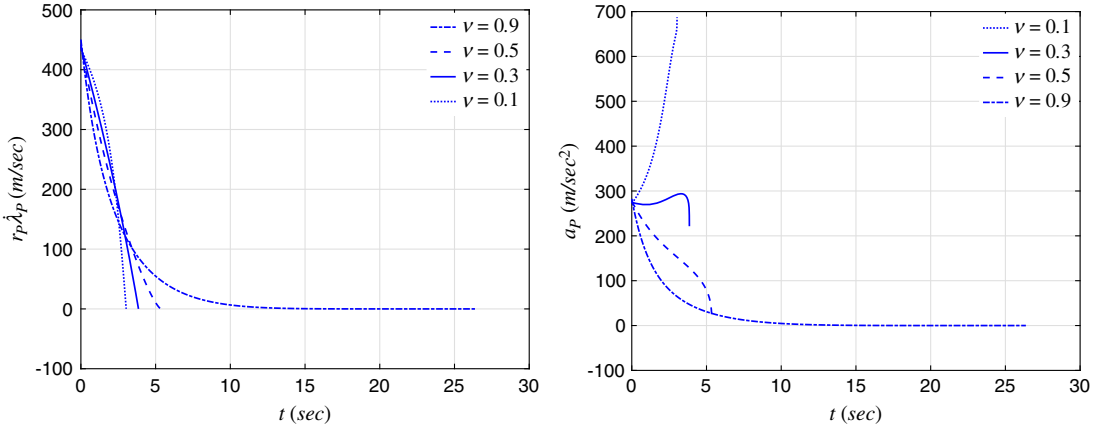

a) Variation of v_λ with time **b) Variation of a_P with time**

Fig. 9 Effect of the variation of ν.

Rearranging the equations gives

$$\dot{v}_r = (v_T \sin\delta_T + v_P \sin\delta_P \cos^2\delta_P)\dot{\lambda}_P \tag{45}$$

$$\dot{v}_\lambda = -(v_T \cos\delta_T + \cos^3\delta_P)\dot{\lambda}_P \tag{46}$$

Let $\nu = v_T/v_P$. Then, the equations can be further rearranged as

$$\dot{v}_r = v_P(\nu \sin\delta_T + \sin\delta_P \cos^2\delta_P)\dot{\lambda}_P \tag{47}$$

$$\dot{v}_\lambda = -v_P(\nu \cos\delta_T + \cos^3\delta_P)\dot{\lambda}_P \tag{48}$$

For a given set of initial conditions, we vary only the parameter ν in the range (0, 1) to see its effect on target capture. Then, the pursuer has a speed advantage over the target. The corresponding plots of v_λ and a_P are given in Figs. 9a and 9b, respectively. Target capture occurs at the point where $v_\lambda = 0$. Figure 9a shows that, as ν increases, v_λ takes more time to become zero. This implies that the capture time t_f increases as v_T approaches v_P. Interestingly, the lateral acceleration a_P changes its nature depending on the value of ν. For smaller values of ν, a_P increases monotonically with respect to time. After a certain critical value of ν, a_P becomes monotonically decreasing with respect to time. Furthermore, for this set of ν values, the engagement ends in a collision triangle as $\dot{\lambda}_P$ becomes zero. The geometrical rule then converges to parallel navigation at target capture.

For $\nu \geq 1$, the target has a speed advantage over the pursuer. Simulation results suggest that the pursuer fails to capture a faster, nonmaneuvering target under the proposed geometrical rule.

For $\dot{\lambda}_P = 0$, Eq. (40) gives

$$v_P \sin\delta_P = v_T \sin\delta_T \tag{49}$$

The geometrical rule gives $\delta_P = \tan^{-1}(\lambda_P - \xi_P)$. After some trigonometric manipulations, we get

$$\sin\delta_P = \frac{\lambda_P - \xi_P}{\sqrt{1 + (\lambda_P - \xi_P)^2}} \tag{50}$$

The substitution of Eq. (50) in Eq. (49) gives

Table 1 Engagement parameters

Parameter	Value
Speed of the pursuer v_P	500 m/s
Speed of the target v_T	0 m/s
Target coordinates (x_T, y_T)	(0, 0)
Initial range r_0	1000 m

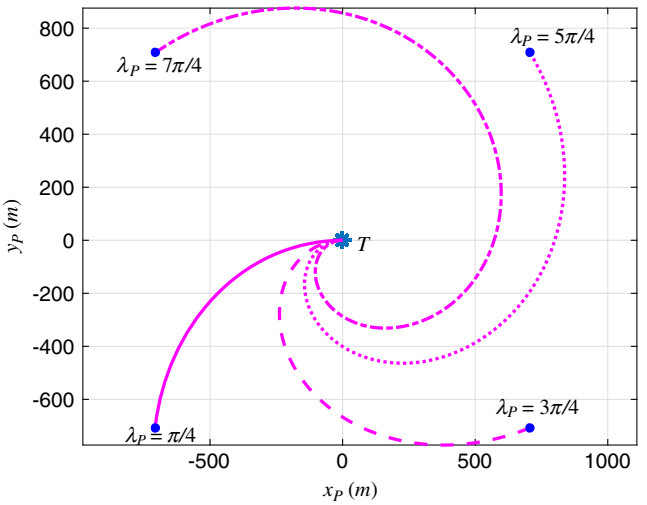

Fig. 10 Trajectories for different initial conditions.

$$v_P \frac{\lambda_P - \xi_P}{\sqrt{1 + (\lambda_P - \xi_P)^2}} = v_T \sin(\gamma_T - \lambda_P) \tag{51}$$

Because the target is moving in a straight-line path, the heading angle γ_T is constant. Thus, Eq. (51) has only one unknown for a given set of initial conditions. The equation can be solved numerically to obtain the final value of $\lambda_P = \lambda_f$. The intercept angle then becomes

$$\gamma_f = \tan^{-1}(\lambda_f - \xi_P) + \lambda_f \tag{52}$$

Thus, the intercept angle is always deviated from the desired value ξ_P by some *a priori* known quantity that could be compensated.

VIII. Simulation Results

This section presents results of numerical simulations to validate the proposed geometrical rule. Throughout this section, the pursuer is assumed to have a constant speed. The target is moving in a straight-line path in one of the cases and is stationary otherwise. To begin with, the initial conditions and the intercept angle of the pursuer are varied, and the effect on the target capturability is studied. The performance of the sliding-mode control-based guidance law is also evaluated. The simulations are carried out in both noise-free and noisy environments for different initial conditions. The scenario where the pursuer has errors in its initial heading angle is also taken into account and evaluated through simulations.

It is to be noted that, in all of the figures obtained through the simulations, the target T and the initial position of the pursuer P are

denoted by an asterisk and a circle, respectively. Also, as mentioned before, the target is assumed to be at the origin.

A. Different Initial Conditions and Intercept Angles

In this subsection, the interception of the target under the geometrical rule proposed in Eq. (7) is simulated for different initial conditions of the pursuer and desired intercept angles. Two types of simulations are carried out; the first considers different initial conditions of the pursuer while the intercept angle remains the same, and the second one has varying intercept angles for the same initial condition of the pursuer. In both the simulations, a noise-free environment is assumed. The engagement parameters that are common in both of the simulations are summarized in Table 1.

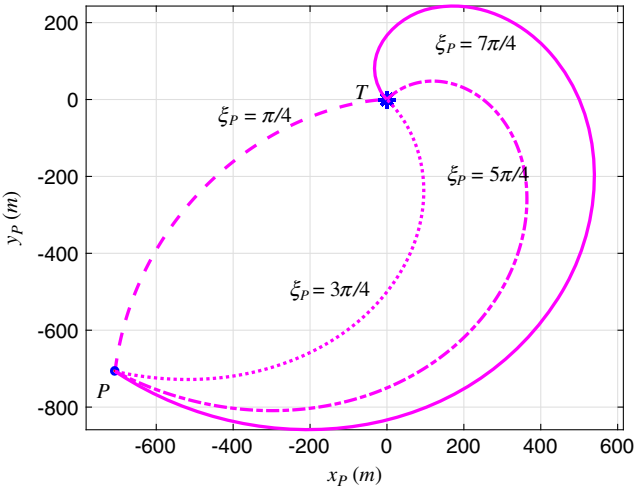

Fig. 11 Trajectories for different intercept angles.

First, we discuss the case when the initial condition of the pursuer is varied while the desired intercept angle is $\xi_P = 0$. Figure 10 shows the trajectories of the pursuer intercepting the stationary target T. The initial line-of-sight angle is different in each case and belongs to the set $\lambda_{P_0} \in \{\pi/4, 3\pi/4, 5\pi/4, 7\pi/4\}$.

It can be noted that when the intercept angle ξ_P, initial range r_0, and line-of-sight angle λ_{P_0} are specified, the parameter a of the resulting spiral is given by $a = (r_0/\lambda_{P_0} - \xi_P)$. The trajectory of the pursuer is governed by the spiral defined by $r_P = (r_0/\lambda_{P_0} - \xi_P)\lambda_P$. The initial lead angle δ_{P_0} is calculated using the geometrical rule given in Eq. (7) and is equal to $\tan^{-1}(\lambda_{P_0} - \xi_P)$. Then, the desired heading angle becomes $\lambda_{P_0} + \tan^{-1}(\lambda_{P_0} - \xi_P)$.

The proposed geometrical rule drives the pursuer to capture the target with the desired intercept angle in all the cases. As we can see, the curvature of the pursuer's trajectory increases as the deviation of the initial line-of-sight angle λ_{P_0} increases from the intercept angle ξ_P. This can be attributed to the decreasing values of the spiral parameter a, as given by Eq. (6), whose effect on the curvature is given by Eq. (28).

Now, we consider the case where the different intercept angles are required to be achieved from the same initial condition of the pursuer. The position coordinate of the pursuer considered for this case is $(r_{P_0}, \lambda_{P_0}) = (1000, \pi/4)$. The simulations are carried out for four different intercept angles that are chosen from the set $\xi_P \in \{0, 3\pi/4, 5\pi/4, 7\pi/4\}$.

Figure 11 shows the trajectories of the pursuer for the different intercept angles. It is clear that the pursuer intercepts the target with the desired intercept angle in each of the cases. Furthermore, the curvature of the pursuer's trajectory varies in accordance with the magnitude of the difference between the line-of-sight angle and the intercept angle, as in the previous case. The higher the difference is,

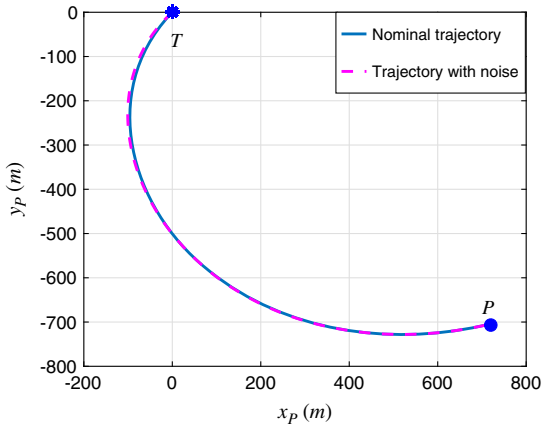

a) Pursuer's trajectory

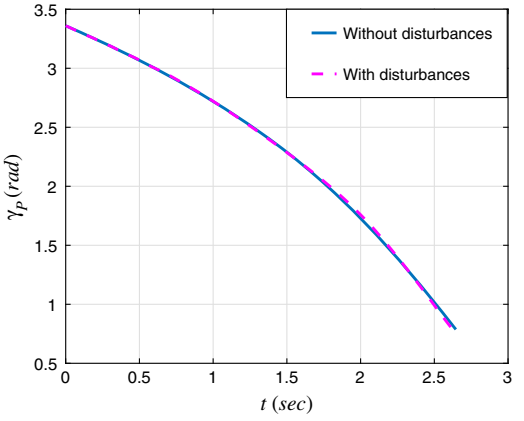

b) Heading angle

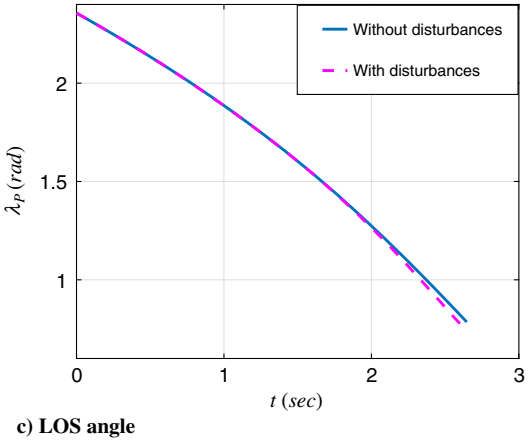

c) LOS angle

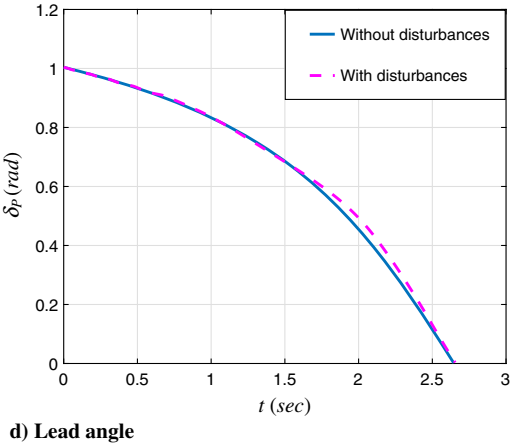

d) Lead angle

Fig. 12 Implementation of the guidance law for a stationary target.

the greater the curvature of the resulting spiral is, and consequently, the higher will be the required terminal lateral acceleration a_P.

B. Guidance Law Implementation

This subsection investigates the robustness of the designed guidance law in the presence of uncertainties. The simulations are carried out for two different scenarios. In the first one, the system is subjected to disturbances, and in the second one, errors in the heading angle of the pursuer are taken into account. In both the cases, the target is assumed to be stationary, and the speed of the pursuer is $v_P = 500$ m/s.

In the first case, the initial range from the stationary target is 1000 m, and the initial line-of-sight angle is $\lambda_P = 3\pi/4$. The desired intercept angle at target capture is equal to $\xi_P = \pi/4$. The disturbances in the system are modeled by $w = 20\sin(t)$. The results achieved through the numerical simulations by using the proposed guidance law are shown in Fig. 12.

Because of the presence of the disturbances, the system behaves like a perturbed system. This can be seen in Fig. 12a, where the trajectory in the presence of disturbances is perturbed with respect to the nominal trajectory. The magnitude of the disturbance w is upper-bounded by 20 m/s^2. Hence, using the results presented in Sec. VI, we set the gain of the uncertainty controller $a_{P\text{un}}$ greater than $\max(|w|) = 20$ as $\beta = 21$.

As proved before, the guidance law drives the dynamics to the sliding surface in finite time, which is clear from Fig. 12. Then, by using the designed guidance law, the pursuer reaches the target at the desired intercept angle in the presence of disturbances. The variations of the heading angle, line-of-sight angle, and lead angle, with respect to time, are shown in Figs. 12b–12d, respectively.

In the second scenario, the performance of the sliding-mode controller is evaluated against errors in the initial heading angle of the pursuer. The nominal trajectory of the pursuer in the absence of any heading error is shown in Fig. 13 in the solid blue line. The heading errors that are used in the simulation lie in the set $\{-\pi/8, -\pi/10, \pi/10, \pi/8\}$. The gain of the sliding-mode controller is chosen as $\beta = 21$.

In all of the cases, the sliding-mode controller drives the pursuer to the target in finite time even in the presence of heading errors. Furthermore, the desired intercept angle is also achieved, as can be seen in the simulation results.

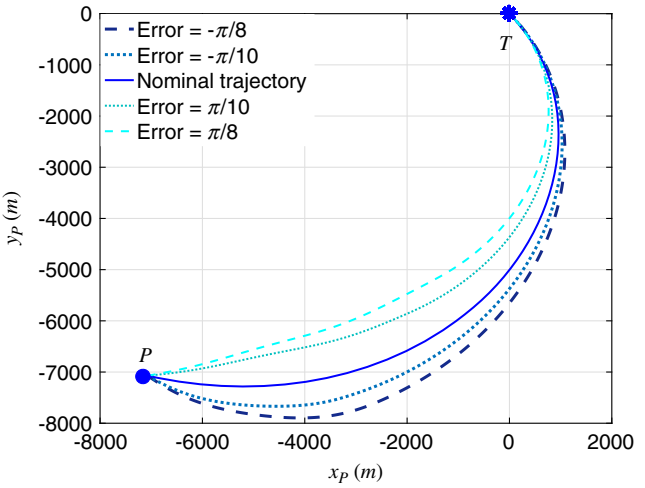

Fig. 13 Robustness against heading errors.

C. Moving Target

In this subsection, we deal with the scenario where the target is moving in a straight-line path. The attributes of the pursuer are $v_P = 500$ m/s, $r_0 = 1000$ m, $\lambda_{P_0} = 0.644$, and $\delta_{P_0} = -1.042$.

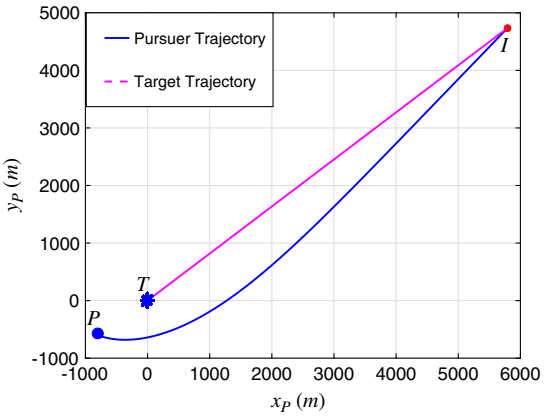

a) Pursuer's trajectory

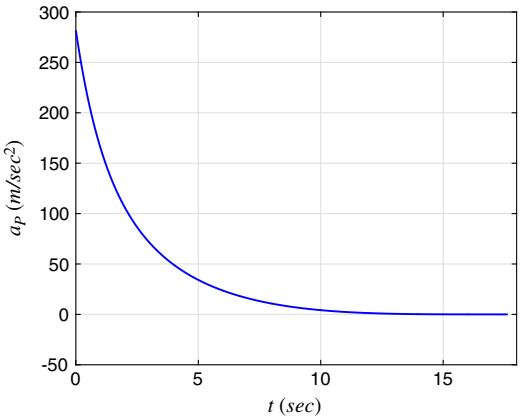

b) Lateral acceleration of the pursuer

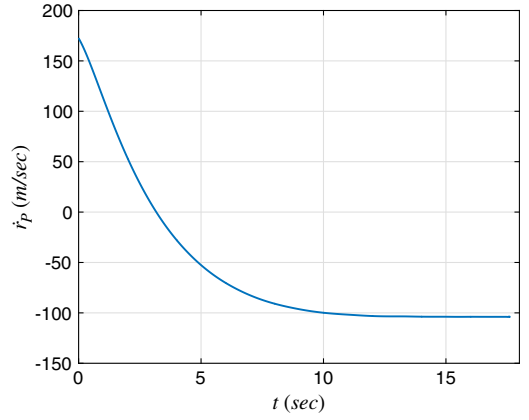

c) Rate of change of r_P

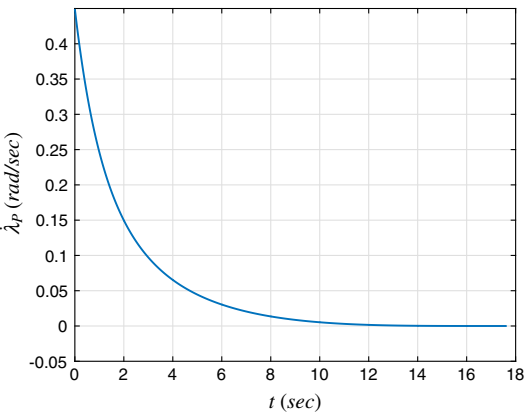

d) Rate of change of λ_P

Fig. 14 Implementation of the guidance law for a moving target.

The parameters of the target are given as $v_T = 425$ m/s, $(x_{T_0}, y_{T_0}) = (0, 0)$, and $\alpha_T = 0.685$. Furthermore, $\xi_P = 3\pi/4$.

Figure 14a shows that the pursuer captures the target at the interception point I even though their speeds are comparable. Furthermore, towards the end of the engagement, the geometrical rule converges to parallel navigation. This can be seen in Fig. 14d, where $\dot{\lambda}_P$ becomes zero after 12 s. Consequently, the engagement ends in a collision triangle. The geometrical rule drives $\dot{r}_P$ from positive to negative values, which in turn drives r_P to zero. During the engagement, the variation of the lateral acceleration a_P is displayed in Fig. 14b. For this particular scenario, a_P reduces monotonically to zero. The actual intercept angle is $\gamma_f = 0.8417$ with a deviation of -1.5145 from the desired intercept angle.

IX. Conclusions

This paper proposes a new geometrical rule, based on an Archimedean spiral, for the interception of stationary targets. As the name suggests, the proposed geometrical rule drives the pursuer along an Archimedean spiral trajectory while enforcing any desired intercept angle. Theoretical results have been presented to prove that interception with a specified intercept angle is guaranteed for any engagement scenario. In scenarios when the initial line-of-sight angle is equal to the desired intercept angle, the pursuer heads toward the target in a straight-line path. When used for a target moving in a straight line, it is observed that the proposed geometrical rule can lead to interception if the pursuer has a speed advantage over the target. It is shown that there exists a deviation between the desired and actual intercept angles, which can be calculated and compensated for a priori.

To implement the proposed geometrical rule, a robust sliding-mode controller is designed. It is proved that the lateral acceleration is always bounded, which makes the implementation of the guidance law feasible in practical scenarios. The implementation is further facilitated by the fact that the guidance law makes use of only angle information. Finally, various numerical simulations are presented in the paper to validate the theoretical results and evaluate the performance of the proposed guidance law in noise-free and noisy environments.

References

[1] Shneydor, N. A., *Missile Guidance and Pursuit: Kinematics, Dynamics and Control*, Woodland, Cambridge, England, U.K., 1998, Chap. 3.

[2] Kim, M., and Kim, Y., "Lyapunov-Based Pursuit Guidance Law with Impact Angle Constraint," *Proceedings of the 19th IFAC World Congress*, IFAC Paper 2509-2514, Cape Town, South Africa, Aug. 2014, pp. 2509–2514. doi:10.3182/20140824-6-za-1003.00233

[3] Livermore, R., and Shima, T., "Deviated Pure-Pursuit-Based Optimal Guidance Law for Imposing Intercept Time and Angle," *Journal of Guidance, Control, and Dynamics*, Vol. 41, No. 8, 2018, pp. 1807–1814. doi:10.2514/1.G003179

[4] Lee, C.-H., Kim, T.-H., and Tahk, M.-J., "Interception Angle Control Guidance Using Proportional Navigation with Error Feedback," *Journal of Guidance, Control, and Dynamics*, Vol. 36, No. 5, 2013, pp. 1556–1561. doi:10.2514/1.58454

[5] Ratnoo, A., and Ghose, D., "Impact Angle Constrained Interception of Stationary Targets," *Journal of Guidance, Control, and Dynamics*, Vol. 31, No. 6, 2008, pp. 1817–1822. doi:10.2514/1.37864

[6] Ratnoo, A., and Ghose, D., "Impact Angle Constrained Guidance Against Nonstationary Nonmaneuvering Targets," *Journal of Guidance, Control, and Dynamics*, Vol. 33, No. 1, 2010, pp. 269–275. doi:10.2514/1.45026

[7] Kim, M., and Grider, K. V., "Terminal Guidance for Impact Attitude Angle Constrained Flight Trajectories," *IEEE Transactions on Aerospace and Electronic Systems*, Vol. 9, No. 6, 1973, pp. 852–859. doi:10.1109/TAES.1973.309659

[8] Ryoo, C.-K., Cho, H., and Tahk, M.-J., "Optimal Guidance Laws with Terminal Impact Angle Constraint," *Journal of Guidance, Control, and Dynamics*, Vol. 28, No. 4, 2005, pp. 724–732. doi:10.2514/1.8392

[9] Shaferman, V., and Shima, T., "Linear Quadratic Guidance Laws for Imposing a Terminal Intercept Angle," *Journal of Guidance, Control, and Dynamics*, Vol. 31, No. 5, 2008, pp. 1400–1412. doi:10.2514/1.32836

[10] Utkin, V. I., *Sliding Modes in Control and Optimization, Communications and Control Engineering*, Springer–Verlag, Berlin, 1992.

[11] Shima, T., "Intercept-Angle Guidance," *Journal of Guidance, Control, and Dynamics*, Vol. 34, No. 2, 2011, pp. 484–492. doi:10.2514/1.51026

[12] Rao, S., and Ghose, D., "Sliding Mode Control Based Terminal Impact Angle Constrained Guidance Laws Using Dual Sliding Surfaces," *12th International Workshop on Variable Structure Systems*, IEEE Publ., Piscataway, NJ, 2012, pp. 325–330. doi:10.1109/VSS.2012.6163523

[13] Harl, N., and Balakrishnan, S., "Impact Time and Angle Guidance with Sliding Mode Control," *IEEE Transactions on Control Systems Technology*, Vol. 20, No. 6, 2012, pp. 1436–1449. doi:10.1109/TCST.2011.2169795

[14] Zhang, Y., Sun, M., and Chen, Z., "Finite-Time Convergent Guidance Law with Impact Angle Constraint Based on Sliding-Mode Control," *Nonlinear Dynamics*, Vol. 70, No. 1, 2012, pp. 619–625. doi:10.1007/s11071-012-0482-3

[15] Kumar, S. R., Rao, S., and Ghose, D., "Sliding-Mode Guidance and Control for All-Aspect Interceptors with Terminal Angle Constraints," *Journal of Guidance, Control, and Dynamics*, Vol. 35, No. 4, 2012, pp. 1230–1246. doi:10.2514/1.55242

[16] Kumar, S. R., Rao, S., and Ghose, D., "Nonsingular Terminal Sliding Mode Guidance with Impact Angle Constraints," *Journal of Guidance, Control, and Dynamics*, Vol. 37, No. 4, 2014, pp. 1114–1130. doi:10.2514/1.62737

[17] Manchester, I. R., and Savkin, A. V., "Circular-Navigation-Guidance Law for Precision Missile/Target Engagements," *Journal of Guidance, Control, and Dynamics*, Vol. 29, No. 2, 2006, pp. 314–320. doi:10.2514/1.13275

[18] Tsalik, R., and Shima, T., "Inscribed Angle Guidance," *Journal of Guidance, Control, and Dynamics*, Vol. 38, No. 1, 2015, pp. 30–40. doi:10.2514/1.G000468

[19] Tsalik, R., and Shima, T., "Inscribed-Angle Guidance Against Moving Targets," *Journal of Guidance, Control, and Dynamics*, Vol. 40, No. 12, 2017, pp. 3211–3225. doi:10.2514/1.G002786

[20] Livermore, R., Tsalik, R., and Shima, T., "Elliptic Guidance," *Journal of Guidance, Control, and Dynamics*, Vol. 41, No. 11, 2018, pp. 2435–2444. doi:10.2514/1.G003565

[21] Chakravarthy, A., and Ghose, D., "Obstacle Avoidance in a Dynamic Environment: A Collision Cone Approach," *IEEE Transactions on Systems, Man, and Cybernetics—Part A: Systems and Humans*, Vol. 28, No. 5, 1998, pp. 562–574. doi:10.1109/3468.709600

[22] Weisstein, E. W., "Archimedes' Spiral," Wolfram Research, Champaign, IL, 2018, http://mathworld.wolfram.com/ArchimedesSpiral.html [retrieved 15 March 2018].

[23] Casey, J., *Exploring Curvature*, Springer Science & Business Media, Wiesbaden, 1996.

[24] Moon, J., Kim, K., and Kim, Y., "Design of Missile Guidance Law via Variable Structure Control," *Journal of Guidance, Control, and Dynamics*, Vol. 24, No. 4, 2001, pp. 659–664. doi:10.2514/2.4792